Conductance Statistics from a Large Array of Sub-10 nm Molecular Junctions

Kacem Smaali,[†,*] Nicolas Clément,[†,*] Gilles Patriarche,[‡] and Dominique Vuillaume[†,*]

[†]IEMN-CNRS, avenue Poincaré, Cité scientifique, Villeneuve d'Ascq, 59652, France and [‡]Laboratoire de Photonique et Nanostructures (LPN), CNRS, route de Nozay, Marcoussis, 91460, France

Controlling and precisely measuring the electronic transport properties through molecular junctions, a crucial issue for the future development of molecular electronics devices, is a long-standing and tricky problem because of the complexity and interplay of several mechanisms such as atomic contact geometry, molecular conformation, and molecule—molecule interactions.[1−3] Statistical methods, using the repetition of hundreds or thousands electrical measurements, are required. Several approaches have been developed, providing a better understanding of transport mechanisms in molecular devices. At the single (or a few) molecule level, using mechanically controllable break junctions (MCBJ) or scanning tunneling microscope MCBJ (STM-MCBJ), several groups have reported multipeak conductance in alkylthiol-based molecular junctions between gold electrodes.[4−12] For instance, a high (HC) and a low (LC) conductance peaks have been observed in the conductance histograms,[4] and several explanations have been proposed related either to the atomistic configuration of the contact geometry (molecule sitting atop a Au adatom or on a hollow site),[4,8] the tilt angle between the molecule and the surface,[13] the different local orientations (*e.g.*, ⟨111⟩ *vs* ⟨100⟩)[14] of the Au surface or the number of molecules. However, there is no consensus. In other studies, three peaks, a single peak, or even no clear peak in the conductance histograms of such alkylthiol junctions are reported.[12,15−17] These discrepancies may come from variabilities of the experimental conditions such as the nature of the solvent (these experiments are performed in a liquid environment), speed at which the MCBJ or STM-NCBJ are operated, data filtering, or selection schemes when used. At a macroscopic level, conductance histograms

ABSTRACT
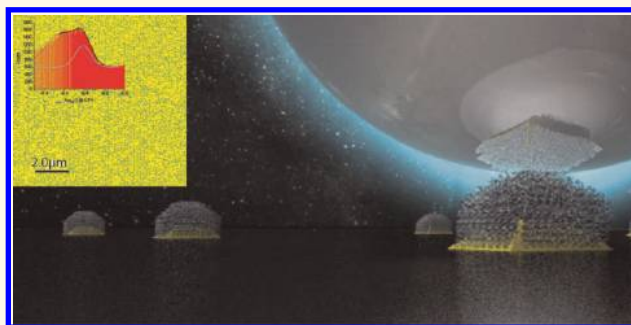
Devices made of few molecules constitute the miniaturization limit that both inorganic and organic-based electronics aspire to reach. However, integration of millions of molecular junctions with less than 100 molecules each has been a long technological challenge requiring well controlled nanometric electrodes. Here we report molecular junctions fabricated on a large array of sub-10 nm single crystal Au nanodots electrodes, a new approach that allows us to measure the conductance of up to a million of junctions in a single conducting atomic force microscope (C-AFM) image. We observe two peaks of conductance for alkylthiol molecules. Tunneling decay constant (β) for alkanethiols, is in the same range as previous studies. Energy position of molecular orbitals, obtained by transient voltage spectroscopy, varies from peak to peak, in correlation with conductance values.

KEYWORDS: molecular electronics · nanodots · nanoelectronics

have also been constructed from measurements with a GaIn eutectic and/or Hg drops, or from measurements on lithographied junctions, albeit with a smaller number of measurements (which are more time-consuming than for MCBJ and STM-MCBJ measurements).[18−25] In these latter cases, due to averaging effect on a large contact area (few μm^2 to mm^2), only a single peak is generally observed in the conductance histograms recorded for molecular junctions with various molecules. At the mesoscopic scale, conductance histogram measurements are scarce. A few groups have reported conductance histograms measured by conducting-atomic force microscope (C-AFM) on self-assembled monolayers (SAM)

on Au surfaces,[23,26,27] albeit many works report only average conductance values. These groups reported a single conductance peak for various molecules (alkylthiols of different lengths, molecular switches) and various measurements conditions.

Here we report a new approach that allows us to measure the conductance of up to a million of junctions in a single C-AFM image. We use molecular junctions fabricated on a large array of sub-10 nm single crystal Au nanodot electrodes, each junction is made of less than one hundred molecules. We focus on alkylthiol junctions as an archetype and for the sake of comparison with an abundant literature for this molecule. We show that the number of the conductance peaks vary, depending on the atomic structure of the electrodes (i.e., single crystal, polycrystal, amorphous). We investigate, using the transition voltage spectroscopy (TVS) method,[29] the electronic structure of junctions belonging to each of the observed conductance population, and we correlate the energy position of the molecular orbitals (with respect to the electrode Fermi energy) with each conductance peak.

RESULTS AND DISCUSSION

Conductance Statistics. We fabricated an array of gold nanodot electrodes by e-beam lithography and lift-off technique (see Methods);[29] each nanodot is covered by a SAM of molecules of interest and contacted by the C-AFM tip (Figure 1a). Since the fabrication and detailed characterization of these nanodot arrays have been reported elsewhere,[29] we recall here the main properties of the nanodots relevant for the molecular conductance measurements. The distance between each nanodot is set to 100 nm. As-fabricated gold nanodots on highly doped silicon are amorphous (Figure 1b). After thermal annealing at 260 °C for 2 h, we obtain a single-crystal gold structure with a flat ⟨100⟩ top surface and a large buried part in contact with the highly doped silicon substrate (Figure 1c). The estimated nanodot diameter from scanning electron microscope (SEM) and high resolution transmission electron microscope (HR TEM) (Figure 1c) is 8 nm (±15%) at the interface with Si and 5 nm (±15%) at the top surface. The height, estimated from atomic force microscope images (Figure 1d and 1e) is 7 nm (±30%). By covering the Au nanodots with SAMs of alkylthiol molecules (C_nH_{2n+1}-SH) referred as C_n with $n = 8, 12$, and 18, we observe an increase of the average height with the number of carbon atoms (Figure 1e) in agreement with the known thickness for such SAMs.[30,31] We estimate that ~80 molecules are sandwiched between the Au nanodots and the C-AFM tip considering a diameter of 5 nm for the top surface and an average molecule coverage of 25 A^2/molecule.[31] This value will be further used to evaluate the conductance per molecule.

By sweeping a C-AFM tip at a given bias, current is measured only when the tip is on top of the molecular junction since conductance of native SiO_2 is below the detection limit of our apparatus (see Supporting Information, movie for a pedagogic presentation of the method). Figure 2 panels a and b show typical C-AFM images taken at −0.4 V and +0.4 V respectively (see Methods) for 1639 amorphous Au nanodot/C_{12}/C-AFM tip molecular junctions. Using a thresholding program (see Methods), we constructed the current histograms shown in Figure 2c for voltages −0.4 V and +0.4 V, respectively. These histograms are well fitted by two log-normal distributions (parameters in Supporting Information, Table S1). In the framework of a nonresonant tunneling transport through the molecular junction, the current is exponentially dependent on the SAM thickness and on the interface energetics (i.e., position of the molecular orbitals relative to the electrode Fermi energy), thus any normal distribution of these parameters leads to a log-normal distribution of the conductance as already observed in molecular junctions.[15,18,20−27] Figure 2d compares current−voltage (I−V) curves reconstructed from the mean current values of histograms measured at various voltages with direct spectroscopic I−V measurements on two molecular junctions selected to belong to the population of the mean of each peak in the histogram (C-AFM tip at a stationary point contact onto the nanojunctions) (see Methods). The very good agreement between the two methods shows that there is no particular influence of tip sweep on current measurements (here, tip scan rate is limited to 3 μm/s). Topographic AFM and C-AFM images of a single Au nanodot covered with C8 molecules and their cross-section profiles are shown in Figure 2e. It is well-known that AFM tip induces a convolution. Therefore, the estimated width from AFM image (~30 nm) is larger than that from SEM or TEM images (~8 ± 2 nm). However, such convolution is much reduced on the C-AFM images (estimated junction diameter, ~15 nm) because the current is proportional to the contact area, which reduces drastically as soon as the tip is moved away from the top of the nanodot.

We measured the current/conductance histograms for molecular junctions made with three different alkyl chains, C_8, C_{12}, and C_{18}, grafted on single-crystal Au nanodots. The current and conductance histograms (conductance normalized to the conductance quantum, G_0 = 77.5 μS, and normalized per molecule considering 80 molecules per dot) taken at 0.2 V are shown in Figure 3a. These histograms are all well fitted with multi-log-normal distributions (see parameters in Table 1 and in Supporting Information Table S2 for C12 and C18). Typical C-AFM images taken at a given force of 7.5 nN for C_8, C_{12}, and C_{18} molecules and related spectroscopic I−V measurements are shown in Supporting Information (Figures S1 −S3). The molecule
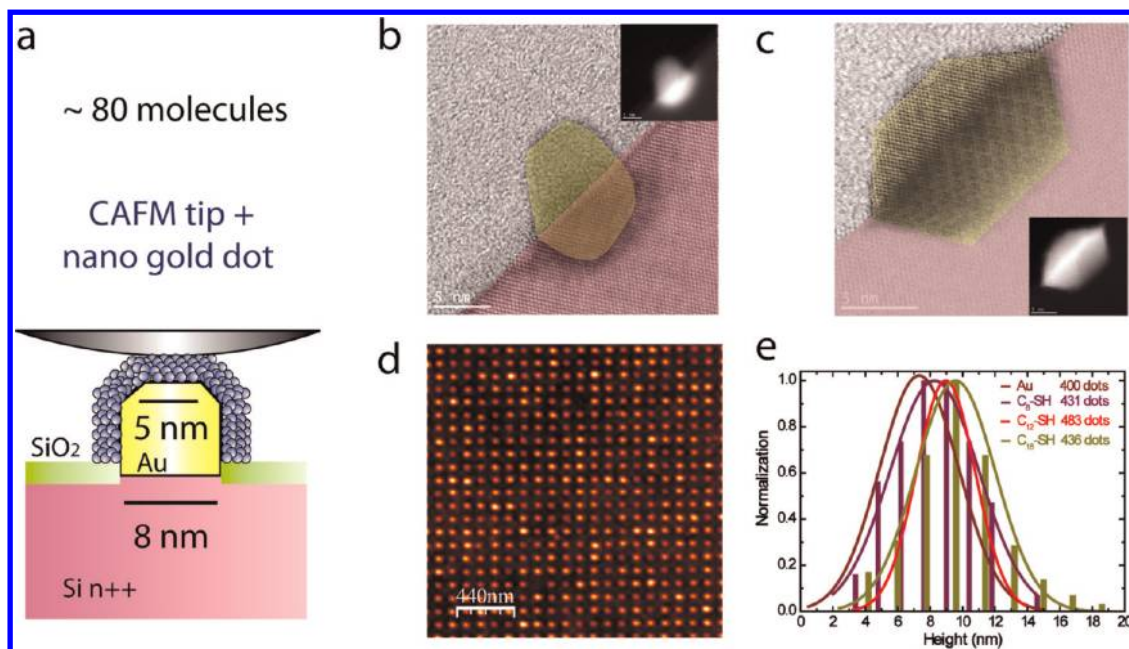
Figure 1. (a) Schematic view of the sub-10 nm molecular junction. Gold nanodots covered by an alkylthiol SAM with ~80 molecules on top are formed on the highly doped n-type Si substrate (resistivity 10^{-3} $\Omega \cdot$cm), while the surface is natively oxidized between nanodots. Molecular junctions are formed when the C-AFM tip is located on top of molecules. (b) STEM image of an amorphous gold nanodot electrode (yellow) on silicon (pink). Inset is the raw image. (c) STEM image of a gold nanodot after annealing at 260 °C for 2 h. (Panels b and c reprinted with permission from ref 29. Copyright 2011 Wiley Publications.) (d) AFM image in tapping mode of an array of gold nanodots covered with C12 molecules (1 μm × 1 μm image with 1024 × 1024 pixels). (e) Normalized height histograms on nanodots and nanodots covered with C8, C12 and C18 molecules.
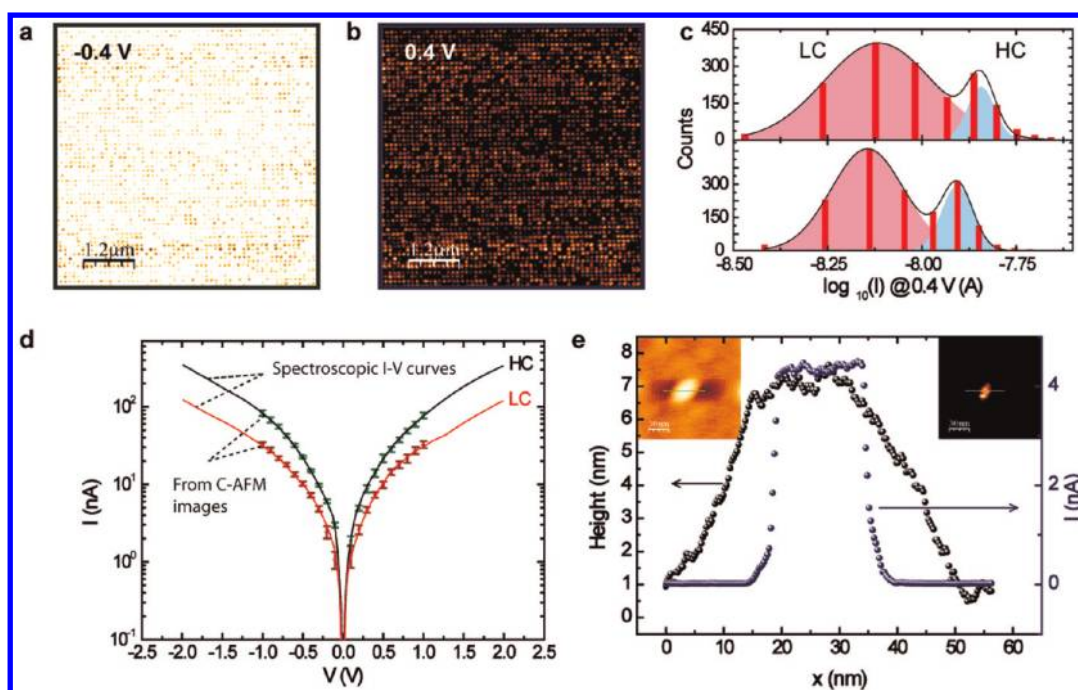

Figure 2. (a,b) C-AFM image at −0.4 V and +0.4 V (voltage applied on the substrate) at a fixed force of 30 nN. (c) Histograms of current obtained from images shown in panels a and b. They are well fitted by two log-normal distributions. (d) $I-V$ curves obtained from histograms and from spectroscopic measurements on representative nanodots belonging of the maximum of each current peak (high conductance, HC, and low conductance, LC) in the histograms. (e) Cross-section view of a single nanodot molecular junction from topographic AFM and C-AFM images shown in insets.

length dependence allows us to determine the tunneling decay constants, β, by plotting the mean

conductance of each peak *versus* the number of carbon atoms in the molecule (Figure 3b) for Au nanodot
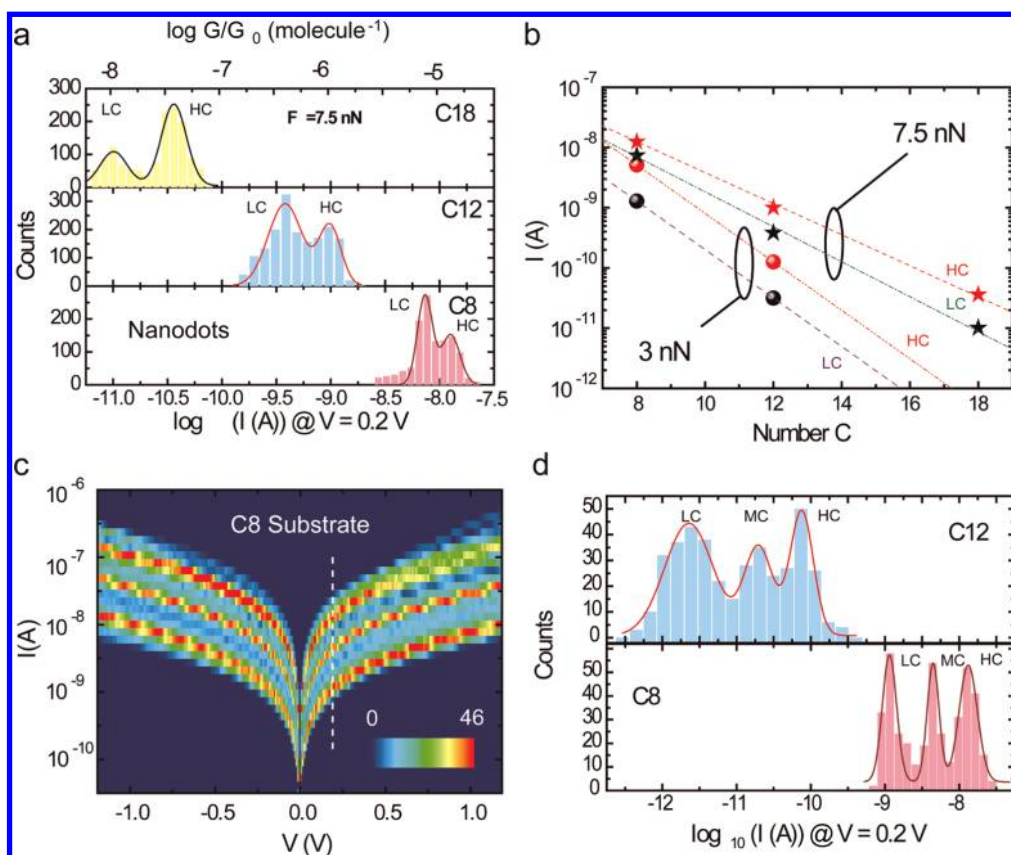
Figure 3. (a) Histograms of the current for the C_8, C_{12}, and C_{18} molecular junctions on a nanodot electrode at a fixed bias of +0.2 V and a loading force of 7.5 nN. (b) Current for each conductance peak *vs* number of carbon atoms for loading forces of 3 nN and 7.5 nN. From these curves, β is extracted. (c) Histograms of the current for the C_8 molecular junctions on Au substrate electrode obtained from 400 spectroscopic $I-V$ curves at a loading force of 30 nN. At a given voltage (*e.g.*, 0.2 V: dashed line) we obtain the histogram shown in panel d for C_8. (d) Histograms of the current for the C_8 and C_{12} molecular junctions on Au substrate electrode at a fixed bias of +0.2 V and a loading force of 30 nN.

TABLE 1. Comparison of Low-Bias (V = 0.2 V) Current (for C8 Molecules), Single Molecule Conductance (in Unit G_0) and β (per Carbon atom) and for Nanodot Junctions (at Two Loading Forces of the C-AFM), Single-Molecule STM-MCBJ Junctions (Literature refs) and Large Au-Substrate Junctions with C-AFM Top Electrode

	nanodots (3 nN)			nanodots (7.5 nN)			single molecule[12]		substrate (30 nN)	
	I (A)	$G(G_0)$ /mol	β (per carbon atom)	I (A)	$G(G_0)$ /mol	β (per carbon atom)	$G(G_0)$ /mol	β (per carbon atom)	I (A)	β (per carbon atom)
HC	5.5×10^{-9}	4.43×10^{-6}	0.9	1.2×10^{-8}	9.7×10^{-6}	0.63	2.8×10^{-4}	1	1.26×10^{-8}	1.33
MC							5.9×10^{-5}	1.04	5×10^{-9}	1.4
LC	1.1×10^{-9}	8.9×10^{-7}	0.9	8×10^{-9}	6.4×10^{-6}	0.74	1.1×10^{-5}	0.95	1.26×10^{-9}	1.57

electrodes (at tip loads of 3 nN and 7.5 nN: see Table 1 and Supporting Information, Figure S4 for histograms at 3 nN). For the sake of comparison with C-AFM measurements on molecular junctions with Au-substrate electrodes (*i.e.*, large lateral size Au film), we also performed $I-V$ measurements (in that case, statistics are obtained from repeated $I-V$ spectroscopic measurements, see Methods) and plotted current histograms (Figure 3c) on molecular junctions with Au-substrate electrode. At a given bias of 0.2 V, we obtained histograms of current (Figure 3d) that can be compared with results obtained for nanodot electrodes

(mean current values and β are given in Table 1). From this set of experiments and representative data from single-molecule junction experiments[12] (Table 1), we deduce several features.

(i) The number of peaks in the current histograms depends on the type of molecular junction. We observed three peaks for Au-substrate electrode, referred to as high conductance (HC), medium conductance (MC), low conductance (LC) and two peaks for Au nanodot electrodes (HC and LC), whereas up to three peaks are observed for single-molecule junctions as mentioned previously.[12] We note that for the Au-substrate electrode,

such a number of conductance peaks reproducibly obtained with several tips and at different loading forces, was not observed in previous C-AFM studies on alkylthiol SAMs on Au.[26,27] This is because we used raw data with a large number of counts (>400) without any averaging/filtering, which can affect the statistics. If we use filtered $I-V$ curves with the same sample and same tip, we get a single peak of current (see Supporting Information, Figure S5). The reduced number of peaks for nanodot electrodes compared to the substrate electrode is consistent with the fact that the nanodot size (5–8 nm) is of the same order of magnitude as (or even smaller than) the known average size for well-organized, close-packed, domains in SAM as measured by grazing-angle X-diffraction (coherence length of the diffraction peak of about 7 nm for C_{18} molecules).[32] In addition, whereas Au nanodots are single crystal, the Au-substrate is polycrystalline, with a larger roughness than the top surface of the Au nanodots. It is likely that the SAMs are more disordered in this case. In all cases, these three peaks are the fingerprint of a worse control on the structural quality of the molecular junctions in that case.

(ii) At low applied loading force (3 nN) β for nanodots ($\sim$0.9 per C, Table 1) is in the same range as results already reported in the literature for molecular junctions by various techniques ($\sim$1 $\pm$ 0.2 per C).[33] It is slightly reduced with increased loading force. β values obtained for the Au-substrate electrode are in the upper range ($\sim$1.4 per C). The loading force used for nanodot electrodes has been reduced compared to that of the substrate electrode since at a given load, the force per surface unit is larger for nanodot electrodes (smaller contact area). Indeed, we have noticed that small β values ($\sim$0.4) are obtained for loads of 30 nN. A detailed study of force dependence including finite element analysis simulation will be reported elsewhere.

(iii) For Au nanodot junctions, the molecular junction area is determined only by the dot size since it is much smaller than the tip radius. Therefore, we can extract the conductance per molecule (considering 80 molecules per dot, see above) and compare with results for single molecule junctions experiments.[12] Our results on nanodots give about 1 order of magnitude lower conductance compared that of to single molecule junctions. We notice a dispersion of conductance/current up to an order of magnitude for measurements on the same sample with several C-AFM tips, which we attribute to dispersion in spring constant (that impact loading force) or atomic shape/roughness of the tip apex, for example. Taking this variability into account, nanodot and single molecule experiments give consistent single molecule conductance values. The current obtained with a substrate electrode is in the same order of magnitude as that for nanodot electrodes, whereas the contact surface is larger. Again, load affects current amplitude and a strict comparison at a given load is difficult given the difference of geometries of electrodes.

(iv) Peak full width half-maximum (fwhm) in log scale is on average $\sim$0.21 for Au nanodots (loading force 7.5 nN). An error of 15% in nanodots diameter leads to an error up to 0.12 in log I, which is below the observed error.

Electronic Structure of Molecular Junctions. To gain insights on the role of molecular organization in the SAMs and to investigate the electronic structure of junctions belonging to each of the observed conductance population, we used the transient voltage spectroscopy (TVS) method.[28,34−37] In this method, the energy barrier height (*i.e.*, the energy offset between the Fermi energy of the metal electrode and one of the molecular orbitals of the molecule) is directly estimated from $I-V$ measurement, by plotting the $I-V$ data in the form of a Fowler−Nordheim plot ($\ln(I/V^2)$ function $1/V$). In the classical interpretation of electron transport through a tunneling barrier,[38] the voltage at which a minimum is observed in this plot represents the transition voltage V_T between the direct and Fowler−Nordheim tunneling regime. Applied to molecular junctions, it was shown that V_T can give an estimation of the energy position of the molecular orbital (relative to the Fermi energy of the electrodes) involved in the transport mechanism, *via* a simple relationship $\varepsilon_0 = \alpha V_T$, where α ($0.8 < \alpha < 2$) depends on several device parameters (symmetry of the junction in particular).[35,36] Albeit, the fact that the exact value of α and the physical origin of V_T are still under debate,[35−37,39] TVS becomes an increasingly popular tool in molecular electronics.[43−46] From direct spectroscopic $I-V$ measurements (Figure 4a) on molecular nanodot junctions (C-AFM tip at a stationary point contact onto the nanodot junctions, see Methods) representative of each conductance peak (*i.e.*, measured on nanodot molecular junctions belonging to the maximum of each peak), we plot $I-V$ curves as Fowler−Nordheim plots (Figure 4b) and get V_{TLC} and V_{THC} for the LC and HC peaks, respectively, at both positive and negative bias. Results are shown in Table 2 for C_8 molecules and in Figure 4c for C_{12} and C_{18}. For all nanodot junctions, the V_T values are in agreement with the previously reported values for alkylthiol junctions (1–1.9 V).[28,34,40] We also note that V_T at positive and negative bias are quite equal (in absolute values), which is related to a symmetric junction[39,41] (*i.e.*, a symmetric coupling of the molecules with the electrodes), in agreement with the symmetric behavior of the $I-V$ curves (Figure 4a). Note that the Pt top electrode and Au bottom electrode have equivalent work function which does not induce asymmetry. As a consequence, based on DFT calculations[36] as well as on analytical modeling[41] we use $\varepsilon_0 = 0.87|V_T|$ to estimate the position of the lowest unoccupied molecular orbital (LUMO). Here, we assume, as recently demonstrated
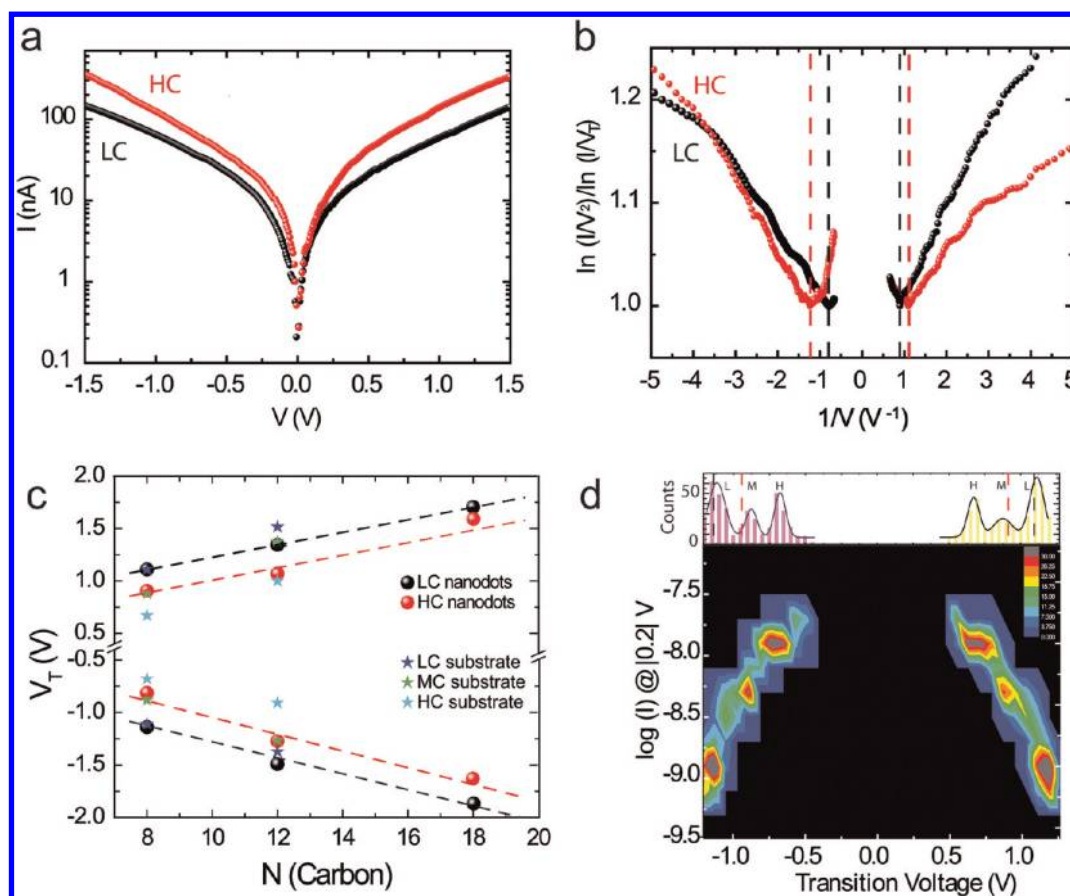
Figure 4. (a) Spectroscopic $I-V$ curves for C_8 molecules performed on two different nanodots representative of the HC and LC peaks (load 7.5 nN). (b) Fowler–Nordheim plots for nanodot electrodes (normalized to 1 at minimum) related to both HC and LC $I-V$ curves shown in panel a. $1/V_T$ for both HC (indicated by dashed black line) and LC (indicated by dashed red line) are obtained from the minimum in each curve. (c) V_T related to each conductance peak for both nanodot and a substrate electrode is plotted as a function of the number of carbon atoms. Black and red dashed lines are guides for eyes. (d) Transition voltage histogram for C_8 on substrate electrode obtained from systematic estimation of $\log(I)@|0.2\ V|$ and V_T for each of the 400 spectroscopic $I-V$ curves. On top is shown 1-D histogram of V_T summing up the counts for all current values (projection on the transition voltage axis of the 2D histogram). Red and black dashed lines indicate V_Ts obtained for both HC and LC peaks on nanodot electrodes suggesting that the HC peak for the substrate electrode is missing for the nanodot electrodes.

TABLE 2. Comparison of the Transition Voltages Measured with Nanodot Junctions (at Two Loading Forces of the C-AFM), Single-Molecule STM-MCBJ Junctions (Literature ref 12) and Large Au-Substrate Junctions with C-AFM Top Electrode for C8 Molecules

	nanodots [@ 7.5 nN (V)]	single molecule (V)[12]		substrate [@ 3 nN (V)]	
C8 HC	−0.813	0.906	−1.49	1.42	−0.68 ± 0.2 0.67 ± 0.2
MC			−1.41	1.4	−0.88 ± 0.2 0.87 ± 0.2
LC	−1.14	1.109	1.12	1.10	−1.12 ± 0.2 1.1 ± 0.2

by UPS and IPES experiments, that electron transport is dominated by the LUMO in the Au/alkylthiol/Au junction.[42] Thus the lower V_T (and ε_0) observed for the HC peak than for the LC one is in agreement with usual electron transport theory,[1] where lower molecule/electrode barrier height leads to higher current. We also observed the same trend for the C12 and C18 nanodot junctions ($I-V$ curves and Fowler–Nordheim plots are shown in Supporting Information, Figure S6). Note that for single-molecule junctions, the peak with

lower V_T was also the peak with lower current.[12] This not intuitive result was explained by a dominant role of contacts in current amplitude, which is not the case in our structure with better controlled contacts. However, we observe a linear increase of both $|V_{THC}|$ and $|V_{TLC}|$ with molecule length (Figure 4c), whereas V_T was observed as constant (within error bars) for single molecule[12] and monolayer-based molecular junctions[28,34,40] but also from theoretical estimation.[35] Such an effect will be discussed in the next paragraph.

To better correlate conductance peaks between nanodot and Au-substrate electrodes, we plot in Figure 4d the V_T histograms (C_8 molecule) *versus* low-bias (at 0.2 V) current measured for about 400 $I-V$ curves taken on the Au-substrate junctions (representative Fowler–Nordheim plots are shown in Supporting Information, Figure S7). Each current peak shown in Figure 3c has a different V_T. As for nanodot electrodes, ther lower the V_T (*i.e.* ε_0) is, the higher is the current. For comparison, we show on the V_T histograms of the Au-substrate junctions (top of Figure 4d), the

average values V_{THC} and V_{TLC} (for both bias) measured on nanodot junctions (Figure 4b). A good match is observed between the LC and MC peaks of the Au-substrate and the LC and HC ones, respectively, for nanodot junctions (see also Figure 4d for chain-length dependence). This could indicate that these peaks have the same origin and that the HC peak for the Au substrate junction is an additional peak, probably due to enhanced disorder in these SAMs. The identification of this HC peak with a more disordered phase in the SAM is in agreement with structural-phase dependency conductance measurements in alkylthiol SAMs on Au, showing a conductance increase with the increase of the average tilt angle (with respect to the surface normal).[42−45] Indeed, the average tilt-angle increases in less-packed, more-disordered, SAMs.[31] Several reasons can explain this conductance increase upon disorder/tilt angle in the SAMs: decrease of the SAMs thickness and thus increase of the tunnel current, increase of the intermolecular chain-to-chain coupling pathway,[42,43] as well as an increase in the conductance of the single Au−S-molecule-tip junction itself due to modification of the Au-molecule interface energetics upon change in the substrate−molecule angle.[14]

We observe a dependence of V_T with alkyl-chain length for both nanodot and substrate electrode. The methodology may play a role since V_T values extracted from filtered spectroscopic curves on substrate electrodes give an almost constant V_T (within error bars: see Supporting Information, Figure S7). In addition, for experiments performed with a C-AFM tip, the load, even though small, may be a source of modification of V_T.[27]

Results obtained with an amorphous nanodot electrode (Supporting Information, Figure S8) lead to a similar level of current compared to that of single-crystal nanodots and similar β values. However, the two peaks of conductance are less clearly distinguished for C_{12} and C_{18} molecules, probably due to dots having a not well-organized monolayer.

Resistive AFM Image on a 1000 × 1000 Dots Array. Previous measurements were taken on about a few thousands of molecular junctions because our C-AFM setup is limited to 512 pixels/image (see Methods). In principle, larger arrays of molecular junctions can be measured. We demonstrate this proof-of-principle by measuring 1 million molecular junctions within a single 100 μm × 100 μm image using other equipment and software (Resistive-AFM, see Methods) with 8192 pixel/image. Figure 5a shows such a resistance-AFM image for a C12 molecular junctions with single-crystal Au nanodot electrodes (zoom on a 40 μm × 40 μm region, for the 100 μm × 100 μm, the nanodots are too small to be visible on the picture). The related histogram from the million molecular junctions is shown in Figure 5b.

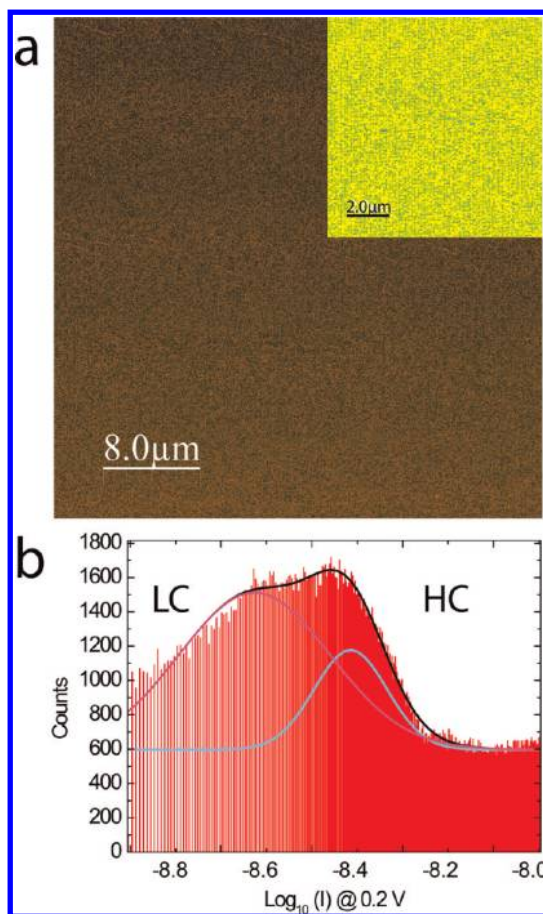The following features are observed. Owing to a minimum scan speed (10 μm/s) imposed by the

Figure 5. (a) The 40 μm × 40 μm image at 30 nN and +0.2 V (voltage applied on the substrate using R-AFM, see Methods) obtained from a zoom of 100 μm × 100 μm image for C_{12} molecular junctions on Au single-crystal electrodes. Inset is a zoom (10 μm × 10 μm). (b) Histograms of the current.

software, we observed pixels with an artifact high current at dot borders (see Supporting Information, Figure S9) which can be partly filtered for histogram construction (inducing a reduction of the total number of counts to 344085). A similar histogram shape is obtained (two peaks) as compared to that of C-AFM measurements with about the same interval/count ratio between the HC and LC peaks (comparison is shown in Supporting Information, Figure S10).

CONCLUSION

Using a large array of sub-10 nm single-crystal Au nanodots as electrode for molecular junctions, we present a new method allowing us to acquire a large amount of conductance data (more than thousands) within a relatively short period of time (time to record one single C-AFM image). For alkylthiol molecules (8 to 18 C atoms), two peaks of conductance are clearly and systematically observed. Conductance per molecule, distance attenuation factor β, and transition voltage V_T are in the same range as previous studies. However, contrary to previous reports, we clearly observe a slight dependence of V_T with alkyl chain length, which may

be related to differences in the statistical data analysis, and/or a peculiar effect of the C-AFM loading force for these nanodot-based molecular junctions. The two conductance peaks are tentatively attributed to different phases of molecular organization in the molecular junctions. These two points deserve further studies.

METHODS

Nanodot Fabrication. For e-beam lithography, we use an EBPG 5000 Plus from Vistec Lithography. The (100) Si substrate (resistivity $=10^{-3}$ $\Omega\cdot$cm) is cleaned with UV-ozone and native oxide etched before resist deposition (same substrate is used for Au-substrate electrode fabrication). The e-beam lithography has been optimized by using a 45 nm-thick diluted (3:5 with anisole) PMMA (950 K). For the writing, we use an acceleration voltage of 100 keV, which reduces proximity effects around the dots, compared to lower voltages. We tried different beam currents to expose the nanodots (100 pA and 1 nA), and we saw no difference in the size of the nanodots as a function of current. So, for the final process, we used 1 nA to optimize exposure time. Then, the conventional resist development/e-beam Au evaporation (8 nm)/lift-off processes are used. Immediately before evaporation, native oxide is removed with dilute HF solution to allow good electrical contact with the substrate. Single crystal Au nanodots can be obtained after thermal annealing at 260 °C during 2 h under N_2 atmosphere. At the end of the process, these nanodots are covered with a thin layer of SiO_2 that is removed by HF at 1% for 1 mn prior to SAM deposition. Spacing between Au nanodots is set to 100 nm. For Au-substrate electrode, 5 nm of Ti and 100 nm of Au are evaporated at 3 Å/s at 10^{-8} Torr.

Self-Assembled Monolayer (SAM). For the SAM deposition, we exposed the freshly evaporated gold surfaces and nanodots to 1 mM solution of alkylthiols (from Aldrich) in ethanol (VLSI grade from Carlo Erba) during 15 h. Then, we rinsed the treated substrates with ethanol followed by a cleaning in an ultrasonic bath of chloroform (99% from Carlo Erba) during 1 min.

C-AFM and R-AFM Measurements. We performed current–voltage measurements by conducting atomic force microscopy (C-AFM) in N_2 atmosphere (Dimension 3100, Veeco), using a PtIr coated tip (same tip for all C-AFM measurements). Tip curvature radius is about 40 nm (estimated by SEM, see Supporting Information, Figure S11), and the force constant is in the range 0.17–0.2 N/m. The C-AFM measurements were taken at loading forces of 3, 7.5, or 30 nN. The conductance of the Au nanodot without molecules is much larger than that for Au nanodots with molecules (Figure S12) and, in that case, dots are often burnt after/during such measurements probably due to the large current density. For larger scan area (100 μm × 100 μm, one million nanodots), we used the resiscope (5600LS Agilent Technologies) with picoview software. This equipment provides the advantages of a large scan ability and large number of pixel per image (up to 8192), but the drawbacks of having an uncalibrated resistance offset (the offset was adjusted from C-AFM measurements) and minimum available scan rate (0.1 Hz) which induces conductance increase at dot borders for large scans (*i.e.*, large speeds >10 μm/s).

Measurements for Au Substrate Electrode. With the placement of the conducting tips at stationary point contact formed nanojunctions, a square grid of 20 × 20 points is defined with a lateral step of 10 nm within a single grain as observed by AFM (see Supporting Information, Figure S13). At each point, only a single $I-V$ curve is acquired and not averaged over many repeated $I-V$ measurements (*e.g.*, 20 curves) since it can affect statistics (Supporting Information, Figure S5). The bias was applied on the Au substrate, and the tip was grounded through the input of the current amplifier. From V_T extraction, each curve is considered independently. When too noisy, curves are not considered for statistics.

Measurements on Gold Nanodots. In the scanning mode, the bias is fixed and the tip sweep frequency is set at 0.5 Hz. In the spectroscopy mode, representative molecular junctions belonging to each conductance peak are first identified from the C-AFM image. Because of imprecise positioning of the tip, 100 spectroscopic $I-V$ curves are taken around this dot using a square grid (10 × 10 points with a lateral step of 2 nm). A significant current can only be measured when the tip is on top of the dot and thus a single $I-V$ (with the maximum current) from these 100 $I-V$ curves is selected per dot.

Number of Counts and Histograms Construction. For Au substrate electrode, we have fixed the number of $I-V$ measurements to 400 because the overall sensed area, with one $I-V$ taken every 10 nm, is within a single grain observed by AFM (see Supporting Information, Figure S13). In addition, estimated data processing time would be 100 times longer than for the array of 3000 molecular junctions. Amorphous Au nanodot electrodes (58%) are often detached from the silicon substrate after the dipping in ethanol and alkyl-thiol solution during the SAM formation. Since our experimental setup is limited to 512 pixels/image, it leads to a typical number of counts of 1460 for a 6 × 6 μm C-AFM image. For annealed Au nanodots, 80% of the nanodots are available (2770 counts). We use our developed OriginC program for threshold analysis (given in Supporting Information). One count corresponds to the maximum current for one nanodot. By using the R-AFM with picoview software (Agilent Technologies), the number of pixels can be increased up to 8192 and the image scan to 100 μm × 100 μm, leading to ~10^6 molecular junctions for 100 nm spacing between dots. Therefore 1 million molecular junctions can be scanned within a single image. For treatment of this huge matrix (8192 × 8192), a computer with >8 GB of RAM is required.

Conflict of Interest: The authors declare no competing financial interest.

REFERENCES AND NOTES

1. Joachim, C.; Ratner, M. A. Molecular Electronics: Some Views on Transport Junctions and Beyond. *Proc. Natl. Acad. Sci. U.S.A.* **2005**, *102*, 8801–8808.
2. Salomon, A.; Cahen, D.; Lindsay, S.; Tomfohr, J.; Engelkes, V. B.; Frisbie, C. D. Comparison of Electronic Transport Measurements on Organic Molecules. *Adv. Mater.* **2003**, *15*, 1881–1890.
3. Vuillaume, D. Molecular Nanoelectronics. *Proc. IEEE* **2010**, *98*, 2111–2123.
4. Li, X.; He, J.; Hihalth, J.; Xu, B.; Lindsay, S. M.; Tao, N. Conductance of Single Alkanethiols: Conduction Mechanism and Effect of Molecule–Electrode Contacts. *J. Am. Chem. Soc.* **2006**, *128*, 2135–2141.
5. Venkataraman, L.; Klare, J. E.; Nuckolls, C.; Hybertsen, M. S.; Steigerwald, M. L. Dependence of Single-Molecular Junction Conductance on Molecular Conformation. *Nature* **2006**, *442*, 904–907.
6. Morita, T.; Lindsay, S. Determination of Single Molecule Conductances of Alkanedithiols by Conducting-Atomic

Force Microscopy with Large Gold Nanoparticles. *J. Am. Chem. Soc.* **2007**, *129*, 7262–7263.

7. Cui, X. D.; Primak, A.; Zarate, X.; Tomfohr, J.; Sankey, O. F.; Moore, A. L.; Moore, T. A.; Gust, D.; Harris, G.; Lindsay, S. M. Reproducible Measurement of Single-Molecule Conductivity. *Science* **2001**, *294*, 571–574.

8. Li, C.; Pobelov, I.; Wandlowski, T.; Bagrets, A.; Arnold, A.; Evers, F. Charge Transport in Single Au/Alkanedithiol/Au Junctions: Coordination Geometries and Conformational Degrees of Freedom. *J. Am. Chem. Soc.* **2008**, *130*, 318–326.

9. Zhou, J.; Chen, F; Xu, B. Fabrication and Electronic Characterization of Single Molecular Junction Devices: A Comprehensive Approach. *J. Am. Chem. Soc.* **2009**, *131*, 10439–10446.

10. Xu, B.; Tao, N. J. *Measurement of Single-Molecule Resistance by Repeated Formation of Molecular Junctions Science* **2003**, *301*, 1221–1223.

11. Haiss, W.; Martin, S.; Scullion, L. E.; Bouffier, L.; Higgins, S. J.; Nichols, R. J. Anomalous Length and Voltage Dependence of Single Molecule Conductance. *Phys. Chem. Chem. Phys.* **2009**, *11*, 10831–10838.

12. Guo, S.; Hihath, J.; Diez-Perez, I.; Tao, N. Measurement and Statistical Analysis of Single-Molecule Current−Voltage Characteristics, Transition Voltage Spectroscopy, and Tunneling Barrier Height. *J. Am. Chem. Soc.* **2011**, *133*, 19189–19197.

13. Haiss, W.; Wang, C.; Grace, I.; Batsanov, A. S.; Schiffrin, D. J.; Higgins, S. J.; Bryce, M. R.; Lambert, C. J.; Nichols, R. J. Precision Control of Single-Molecule Electrical Junctions. *Nat. Mater.* **2006**, *5*, 995–1002.

14. Sen, A.; Kaun, C.-C. Effect of Electrode Orientations on Charge Transport in Alkanedithiol Single-Molecule Junctions. *ACS Nano* **2010**, *4*, 6404–6408.

15. Gonzalez, M. T.; Wu, S.; Huber, R.; van der Molen, S. J.; Schonenberger, C.; Calame, M. Electrical Conductance of Molecular Junctions by a Robust Statistical Analysis. *Nano Lett.* **2006**, *6*, 2238–2242.

16. Ulrich, J.; Esrail, D.; Pontius, W.; Venkataraman, L.; Millar, D.; Doerrer, L. H. Variability of Conductance in Molecular Junctions. *J. Phys. Chem. B* **2006**, *110*, 2462–2466.

17. Venkataraman, L.; Klare, J. E.; Tam, I. W.; Nuckolls, C.; Hybertsen, M. S.; Steigerwald, M. L. Single-Molecule Circuits with Well-Defined Molecular Conductance. *Nano Lett.* **2006**, *6*, 458–462.

18. Chiechi, R. C.; Weiss, E. A.; Dickey, M. D; Whitesides, G. M Eutectic Gallium−Indium (EGaIn): A Moldable Liquid Metal for Electrical Characterization of Self-Assembled Monolayers. *Angew. Chem., Int. Ed.* **2008**, *47*, 142–144.

19. Holmlin, R. E.; Haag, R.; Chabinyc, M. L.; Ismagilov, R. F.; Cohen, A. E.; Terfort, A; Rampi, M. A.; Whitesides, G. M. Electron Transport through Thin Organic Films in Metal−Insulator−Metal Junctions based on Self-Assembled Monolayers. *J. Am. Chem. Soc.* **2001**, *123*, 5075–5085.

20. Nijhuis, C. A.; Reus, W. F; Whitesides, G. M. Molecular Rectification in Metal−SAM−Metal Oxide−Metal Junctions. *J. Am. Chem. Soc.* **2009**, *131*, 17814–17827.

21. Nijhuis, C. A.; Reus, W. F.; Whitesides, G. M. Mechanism of Rectification in Tunneling Junctions Based on Molecules with Asymmetric Potential Drops. *J. Am. Chem. Soc.* **2010**, *132*, 18386–18401.

22. Thuo, M. M.; Reus, W. F.; Nijhuis, C. A.; Barber, J. R.; Kim, C.; Schulz, D.; Whitesides, G. M. Odd-Even Effects in Charge Transport across Self-Assembled Monolayers. *J. Am. Chem. Soc.* **2011**, *133*, 2962–2975.

23. Smaali, K.; Lenfant, S.; Karpe, S.; Ocafrain, M.; Blanchard, P.; Deresmes, D.; Godey, S.; Rochefort, A.; Roncali, J.; Vuillaume, D. High On-Off Conductance Switching Ratio in Optically-Driven Self-Assembled Conjugated Molecular Systems. *ACS Nano* **2010**, *4*, 2411–2421.

24. Kim, T.-W.; Wang, G.; Lee, H.; Lee, T. Statistical Analysis of Electronic Properties of Alkanethiols in Metal−Molecule−Metal Junctions. *Nanotechnology* **2007**, *18*, 315204–315211.

25. Wang, G.; Kim, T.-W.; Lee, H.; Lee, T. Influence of Metal−Molecule Contacts on Decay Coefficients and Specific Contact Resistances in Molecular Junctions. *Phys. Rev. B* **2007**, *76*, 205320–205325.

26. Engelkes, V. B.; Beebe, J. M.; Frisbie, C. D. Analysis of the Causes of Variance in Resistance Measurements on Metal−Molecule−Metal Junctions Formed by Conducting-Probe Atomic Force Microscopy. *J. Phys. Chem. B* **2005**, *109*, 16801–16810.

27. Wang, G.; Kim, T.-W.; Jo, G.; Lee, T. Enhancement of Field Emission Transport by Molecular Tilt Configuration in Metal−Molecule−Metal Junctions. *J. Am. Chem. Soc.* **2009**, *131*, 5980–5985.

28. Beebe, J. M.; Kim, B.; Gadzuk, J. W.; Frisbie, C. D.; Kushmerick, J. G. Transition from Direct Tunneling to Field Emission in Metal−Molecule−Metal Junctions. *Phys. Rev. Lett.* **2006**, *97*, 026801–026804.

29. Clément, N.; Patriarche, G.; Smaali, K.; Vaurette, F.; Nishiguchi, K.; Troadec, D.; Fujiwara, A.; Vuillaume, D. Large Array of Sub-10 nm Single-Grain Au Nanodots for Use in Nanotechnology. *Small* **2011**, *7*, 2607–2613.

30. Porter, M. D.; Bright, T. B.; Allara, D. L.; Chidsey, C. E. D. Spontaneously Organized Molecular Assemblies. Structural characterization of *n*-alkyl Thiol Monolayers on Gold by Optical Ellipsometry, Infrared Spectroscopy and Electrochemistry. *J. Am. Chem. Soc.* **1987**, *109*, 3559–3568.

31. Ulman, A. *An Introduction to Ultrathin Organic Films: From Langmuir−Blodgett to Self-Assembly*; Academic Press: San Diego, CA, 1991.

32. Maoz, R.; Sagiv, J.; Degenhardt, D.; Quint, M. M. Hydrogen-Bonded Multilayers of Self-Assembling Silanes: Structure Elucidation by Combined Fourier Transform Infrared Spectroscopy and X-ray Scattering Techniques. *Supramol. Sci.* **1995**, *2*, 9–24.

33. Salomon, A.; Cahen, D.; Linsay, S.; Tomfohr, J.; Engelkes, V. B.; Frisbie, C. D. Comparison of Electronic Transport Measurement on Organic Molecules. *Adv. Mater.* **2003**, *15*, 1881–1890.

34. Beebe, J. M.; Kim, B.; Frisbie, C. D; Kushmerick, J. G. Measuring Relative Barrier Heights in Molecular Electronic Junctions with Transition Voltage Spectroscopy. *ACS Nano* **2008**, *2*, 827–832.

35. Huisman, E. H.; Guédon, C. M.; van Wees, B. J.; van der Molen, S. J. Interpretation of Transition Voltage Spectroscopy. *Nano Lett.* **2009**, *9*, 3909–3913.

36. Chen, J.; Markussen, T.; Thygesen, K. S. Quantifying Transition Voltage Spectroscopy of Molecular Junctions: *Ab Initio* Calculations. *Phys. Rev. B* **2010**, *82*, 121412–121415.

37. Markussen, T.; Chen, J.; Thygesen, K. S. Improving Transition Voltage Spectroscopy of Molecular Junctions. *Phys. Rev. B* **2011**, *83*, 155407–155412.

38. Simmons, J. G. Generalized Formula for the Electric Tunnel Effect between Similar Electrodes Separated by a Thin Insulating Film. *J. Appl. Phys.* **1963**, *34*, 1793–1803.

39. Mirsani, F.; Thijssen, J.; van der Molen, S. J. Advantages and Limitations of Transition Voltage Spectroscopy: A Theoretical Analysis. *Phys. Rev. B* **2011**, *84*, 115402–115409.

40. Song, H.; Kim, Y.; Jeong, H.; Reed, M. A.; Lee, T. K. *J. Phys. Chem. C* **2010**, *114*, 20431–20435.

41. Baldea, I. Ambipolar Transition Voltage Spectroscopy: Analytical Results and Experimental Agreements. *Phys. Rev. B* **2012**, *85*, 035442–0354446.

42. Qi, Y.; Yaffe, O.; Tirosh, E.; Vilan, A.; Cahen, D.; Kahn, A. *Chem. Phys. Lett.* **2011**, *511*, 344–347.

43. Song, H.; Lee, H.; Lee, T. Intermolecular Chain-to-Chain Tunneling in Metal, Alkanethiol, Metal Junctions. *J. Am. Chem. Soc.* **2007**, *129*, 3806–3807.

44. Yamamoto, H.; Waldeck, D. H. Effect of Tilt-Angle on Electron Tunneling through Organic Monolayer Films. *J. Phys. Chem. B* **2002**, *106*, 7469–7473.

45. Qi, Y.; Ratera, I.; Park, J. Y.; Ashby, P. D.; Quek, S.-Y.; Neaton, J. B.; Salmeron, M. Mechanical and Charge Transport Properties of Alkanethiol Self-Assembled Monolayers on a Au(111) Surface: The Role of Molecular Tilt. *Langmuir* **2008**, *24*, 2219–2223.